# CHAPTER IV

# IMPLICATIONS OF NATURAL AND SYNTHETIC INHIBITORS TO MITIGATE CORROSION IN STEEL REBAR ENTRENCHED IN CONCRETE

## 4.1 Introduction

In recent years, steel rebar has been the widely used material for constructions and other infrastructural activities due to their reliability, durability, versatility and acceptability[1,2]. It acts as a tensioning device to bolster concrete and also assists in holding the concrete during a compressed state. It can be bent facilely and sited in concrete to form a monolithic structure[3]. Thermal expansion property and outstanding bendability makes steel rebar as an excellent material for the reinforcement in concrete structures. Concrete is a material that is tough in compression but not as effective in strength. In order to balance the disparities, steel rebar is embedded in concrete to withstand the high load. The steel rebar is designed in such a way that it provides an improved bond with concrete. Concrete affords unswerving protection against corrosion. Due to insufficiency of understanding the condition of the environment, the steel rebar is not able to withstand in strength up to the expected level. In RCC (Reinforced Cement Concrete), steel rebar is used which supports the concrete but on the other side it spoils the permanence, endurance of concrete due to adverse effects of corrosion. Among the numerous factors accountable for the damage of steel rebar in concrete, corrosion is the significant one. In fact, it is tagged as "Cancer" for concrete[4]. The ideal expected life of RCC is about hundred years. But in practice, it lasts around 20 to 25 years due to severe damage and perturbation[5]. It is assessed that cost for substituting (or) refurbishing the damaged structure worldwide is approximately more than $20 billion per year and it is increasing at the rate of additional $500 million per year[6]. The usage of TMT bars (Thermo mechanically treated rebars) emerged in 80s. It is a superior material of high strength of around 510 to 590 Mpa (megapascal). But it is easily susceptible to corrosion. It is identified that the steel rebar corrosion has a huge economic loss and other social implications on society and also threatens the life of the people who are involved in the construction activities by means of corrosion damaging the structure. Even in an efficient construction, corrosion initiated due to ingress of chloride into the

concrete results in the attack of the passive film of the steel rebar[7]. It is very important to understand the susceptibilities of concrete structures to reduce maintenance cost and long term repair. We know that de-icing chemicals and seawater are the two major sources containing chlorides[8]. Most of the bridges that are constructed nearby coastal region are more prone to corrosion because of the influence of sea water. Chloride acts as a catalyst for corrosion to occur. In the presence of oxygen, iron atoms dissolve as ferrous ions and get precipitated as ferric oxides and these oxides occupy more volume than the volume of the original steel rebar ensuing in the delamination, stresses, formation of cracks and spalling the concrete cover[9]. The following are the characteristics of efficient steel rebar which indeed can reduce corrosion:

- Higher strength
- Good holding capacity with concrete
- High Thermal expansion
- Good bearing capacity to natural disasters
- Easy to shape
- Better cage binding
- Claiming corrosion delay

### 4.1.1 Role of chloride ions and carbon dioxide in corrosion

Several approaches have been made in order to elucidate the role of chloride ions in promoting corrosion. Chloride ion attacks the steel rebar through cracks (or) penetration in concrete. In order to explain the attack of chloride ion various theories were proposed by researchers as shown below[10].

- Oxide film theory states that the passive oxide film destroyed due to chloride ions, depassivation takes place and corrosion gets initiated.
- Adsorption theory specifies that adsorption of chloride ion on the rebar surface takes place thus confronting the steel.

- Transition complex theory proposes that chloride ion act as a catalyst. Grouping of the chloride ion with ferrous ion has a tendency to form a soluble iron chloride complex. These complexes may give out chloride ion and ferrous hydroxide. This results in the formation of rust as shown in the below reactions,

**Step 1: Formation of intermediate soluble iron chloride**

Chloride ion reacts with $Fe^{2+}$ forming an iron-chloride complex.

$$Fe + 2\ Cl^- \longrightarrow [Fe^{2+} + 2Cl^-] + 2e^-$$

**Step 2: Formation of ferrous hydroxide**

Iron chloride complex thus obtained from the subsequent previous reaction hydrolyses and gives ferrous hydroxide with the liberation of chloride ions which has a tendency to attack the iron surface[11].

$$[Fe^{2+} + 2Cl^-] + 2H_2O + 2e^- \longrightarrow Fe(OH)_2 + 2H^+ + 2Cl^-$$

**Step 3: Formation of hydrogen gas**

Hydrogen ion get reduced to hydrogen gas

$$2H^+ + 2e^- \longrightarrow H_2$$

**Step 4: Formation of rust**

Ferrous hydroxide in presence of moisture and air resulting in the formation of rust

$$4Fe(OH)_2 + O_2 + 2H_2O \longrightarrow 4Fe(OH)_3$$

Rust produced during corrosion process occupies a volume equivalent to 4 - 6 times than initial steel. This greater volume induces stress in the concrete, forming cracks through which water and chloride reaches the steel rebar. Carbon dioxide reaches the concrete and get dissolved in pore solution and carbonic acid is formed. The carbonic acid reacts with alkaline medium available in the cement forming carbonates thus lowering the pH level of the concrete. At a particular period of time alkalinity attains low pH level due to the formation of calcium carbonate and thus in the existence of oxygen and water depassivation

of steel rebar takes place thus instigating corrosion[12]. In general, pH of the pore solution is between 12 -13 but due to carbonation process pH decreases reaching around less than 9.5 thus ensuing corrosion[13].

$$CO_2 + H_2O \longrightarrow H_2CO_3$$

$$H_2CO_3 + Ca(OH)_2 \longrightarrow CaCO_3 + 2H_2O$$

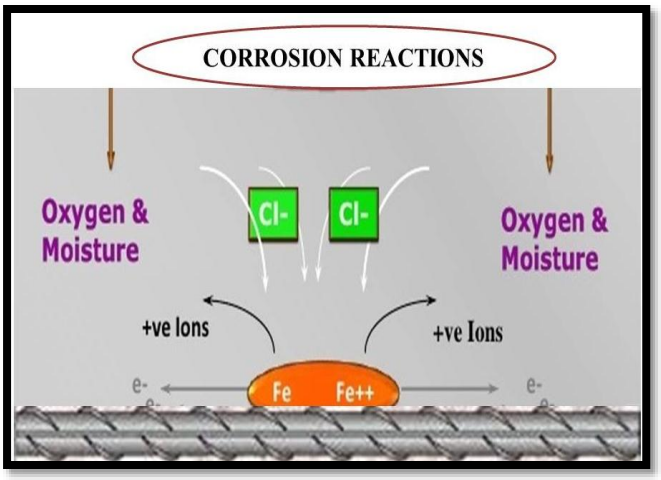


**Fig. a: Corrosion reactions in presence of chloride ion**

### 4.1.2 Process of corrosion in steel rebar

Rebar corrosion in concrete is an electrochemical process were electrochemical cells are created in the following ways[14],

- two dissimilar metals such as steel rebars, aluminium pipes implanted in concrete (or) change in surface characteristics of steel in composition cell
- due to the differences in the concentration of alkali and chlorides ensuing in the formation of concentration cells

Parameters such as oxygen and moisture involved in initiating the corrosion are the main components responsible for corrosion. Corrosion process is highly influenced by oxygen and water. Severe pitting corrosion is observed on the rebar surface even at low oxygen level producing corrosion products. Furthermore, it can also be noticed visibly on the surface leading to quick loss in the load bearing capacity of the concrete. Chloride ion is an important reason for corrosion process in steel[15]. It can easily penetrate through the

pores and attack the passive film of the steel. It has been suggested by some of the authors that degradation of film depends on the concentration of chloride and hydroxide ion. Moisture content act as an electrolyte and area that is nearer to chloride ion act as cathode thus facilitating the electrochemical process. Chloride can take up two forms in concrete that is bound chloride and free chloride. Bound chloride is chemically bound and it is used as hydration product in cement, whereas physically bound chloride gets physically adsorbed on the pores of the gel surface. Free chlorides are pertinent for corrosion to occur in steel.

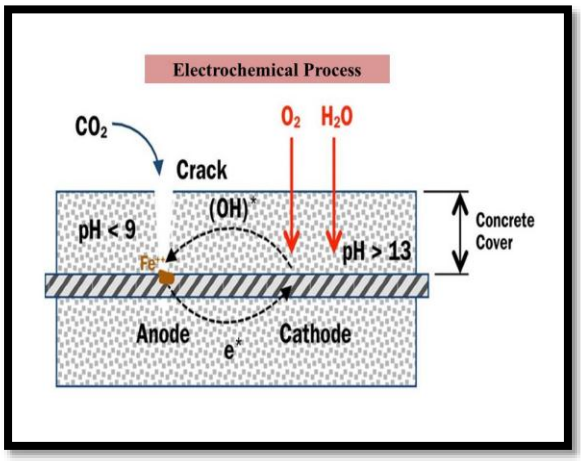


**Fig. b: Formation of cracks due to $CO_2$**

### 4.1.3 Signs of corrosion in steel rebar

The vulnerable activity of corrosion deteriorates the physical look of the structure as well as strength, durability leading to reduction in cross sectional area of the steel. The damage of steel due to corrosion occurs in the following stages[16].

Stage 1: generation of white patches due to carbonation process

Stage 2: brown iron oxide layer is formed along the steel bar

Stage 3: cracks are formed due to high pressure on the concrete

Stage 4: loss of bond created between the concrete and steel rebar leads to spalling

Stage 5: reduction in the size of steel rebar

Stage 6: Bulging of concrete leads to buckling of bars

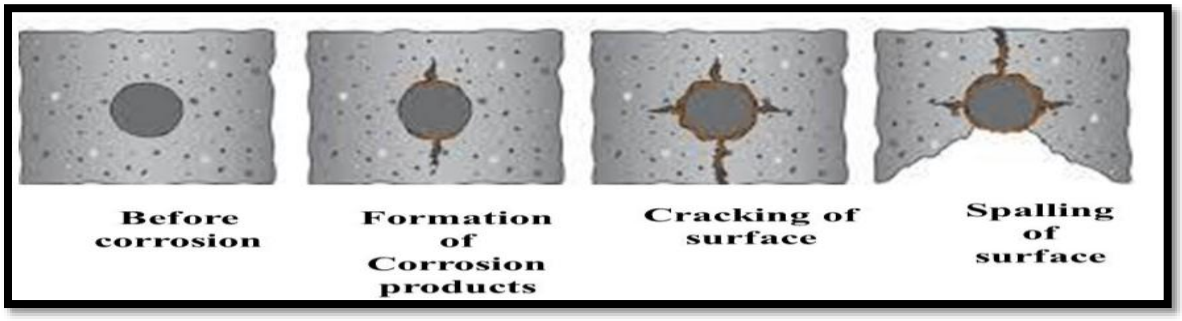


**Fig. c: Effects of corrosion**

### 4.1.4 Curtailing the risk of corrosion

Corrosion control is the focal solution in order to preclude impairment and failure of concrete structures entrenched in steel rebar. Approximately 40% of concrete fiasco is due to the vulnerable effect of corrosion. To diminish the chances of formation of corrosion products several methods are available such as cathodic protection, coatings, galvanisation electrochemical chloride extraction, electrochemical chloride migration, realkalisation encapsulation of fibre reinforced polymers and corrosion inhibitors[17,18]. Out of all these methods inhibitors play a remarkable role in mitigating corrosion. Virtually, an inhibitor has a tendency to adsorb on the metal surface thus shielding the metal from corrosion. Inhibitor can be used in the form of solution (or) powder for coating. An inhibitor is active if they satisfy some criteria like long term stability, uniform distribution, not to leach out from concrete and do not amend the properties of concrete. Inhibitor prevents corrosion in the following ways

- induce cathodic or anodic polarisation behaviour at low current values
- reducing the diffusion of ions to the surface of the metal
- electrical resistance of the metal gets increased

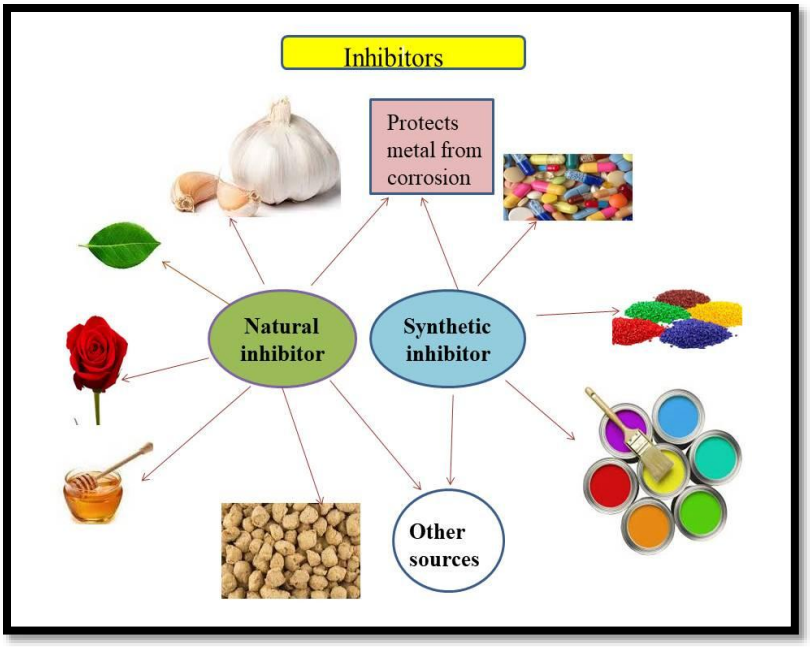


**Fig. d: Sources of corrosion**

Natural and synthetic inhibitors can be used to guard the metal from corrosion. The biocompatible phytochemical components existing in the plant extracts are rich in lone pairs, aromatic rings and π-electrons. Hence they interact with anodic/cathodic reactions resulting in the blockage of active sites by eliminating water molecules thus leading to the creation of protective layer on the metal surface by adsorption process on metal/electrolyte interface there by decreasing the rate of corrosion[19,20]. Synthetic inhibitors contain electro active nitrogen, sulphur, oxygen atoms, aromatic rings which form complexes with metal impeding the dissolution of the metal. Research work associated with the usage of inhibitors for rebar corrosion has been reported in literature. A detailed review of literature was made and it is described below.

## 4.2 Review of literature

**Eyu *et al.*,** studied the comparative analysis of *Vernonia amygdalina*, calcium nitrite and sodium nitrite inhibition on carbon steel entrenched in concrete by electrochemical and weight loss test exposed to simulated marine chloride environment. The specimen was exposed to NaCl solution and the concrete resistivity and corrosion potential were experimented. On visual examination of specimen, pitting corrosion was detected in the

specimens without inhibitor. The results indicated that natural inhibitor reduced the corrosion rate much better than sodium nitrite. The layer was physically adsorbed thus guarding the metal from corrosive environment[21].

Anti-corrosive property of green *Bambusa Arundinacea* leaves was carried out by **Asipita *et al.*,.** by using compressive strength test, field emission scanning electron microscopy and durability test by exposing the specimen for 360 days. The efficiency of the green inhibitor was compared with inhibitors such as calcium nitrite and ethanol amine. Results revealed that water absorption values of the metal decreases as the time increases. KOH in the concrete acted as a chemical water barrier and reduced the permeability of chloride ion thus protecting the metal from corrosion[22].

The corrosion inhibition performance of sorbitol on steel rebar was evaluated by **Feng *et al.*,** by EIS and polarisation methods. The specimen was exposed in the simulated pore solution to accelerate corrosion. It has been found that anodic and cathodic reactions can be curbed by inhibitor. Sorbitol has a tendency to adsorb on the metal surface resulting in the formation of passive layer. Results specified that sorbitol have affinity to inhibit corrosion[23].

A study on anti-corrosive property of urea fertiliser - $Sn^{2+}$and $Zn^{2+}$ system on reinforced steel in 3% NaCl was carried out by **Mahadi *et al.*,** by potentiodynamic polarisation and cyclic voltammetry methods. Polarisation showed an inhibition efficiency of 85.9% for 300 ppm of urea and 50 ppm of $Sn^{2+}$, where as 82.4% was attained for the concentration of 300 ppm of urea and 50 ppm of $Zn^{2+}$. Cyclic voltammetry exposed that pitting corrosion was reduced to a greater extent in presence of inhibitor. It has been observed that urea - $Sn^{2+}$ inhibitor was able to maintain a stable layer on the metal surface thus indicating better inhibitor in comparison with urea - $Zn^{2+}$ [24].

A comparative approach for protecting reinforced steel from corrosion using amino alcohol and lithium nitrite inhibitors were assessed by **Lee *et al.*,** by electrochemical testing methods. Reinforced steel and concrete specimens were exposed in simulated chloride environment. $LiNO_2$ inhibitor of concentration of 25% and amino alcohol of 80% were used. It has been observed from the results that $LiNO_2$ displayed a superior inhibitive property than amino alcohol[25].

**Cherif *et al*.,** studied corrosion inhibition behaviour of tannins on steel entrenched in carbonated concrete by techniques such as EIS, linear polarisation resistance and potentiodynamic polarisation techniques. From the results it was concluded that formation of dense film on the reinforced steel provided cathodic protection and enhanced corrosion resistance[26].

Corrosion inhibition performance of *Morinda Lucida* on steel in simulated industrial-microbial environment was implemented by **Okeniyi *et al*.,** in 0.5 M $H_2SO_4$ medium. Inhibition efficiency of 98.76% was attained at a concentration of 0.416% of inhibitor where as 93% of efficiency was attained for 0.3333% of inhibitor concentration indicating that rise in concentration increases the protection efficiency. The effectiveness of extract was analysed at different concentrations by electrochemical monitoring techniques using steel-reinforced concrete specimens in acid medium[27].

**Okeniyi *et al*.,** evaluated the influence of *Phyllanthus muellerianus* leaf extract on steel in 3.5% NaCl by electrochemical methods. The experimental data was statistically analysed and data provided an excellent correlation with function of concentration and noise resistance. The maximum protection efficiency attained was 97.5% for 0.3333% of the extract admixture in saline/marine test environment. Theoretical and experimental model followed Langmuir adsorption isotherm. The adsorption process was spontaneous and layer was physically adsorbed on the metal surface. It has been found that the inhibition performance was due to the existence of S, N, O and π- electrons[28].

Corrosion preventive technique was assessed by **Abdul *et al*.,** using rice husks as inhibitor in 3.5% NaCl. Concrete samples were prepared, it was analysed for mechanical testing and performance of the inhibitor was scrutinized by electrochemical corrosion method. Efficacy was analysed at different concentrations of powdered rice husks (1%, 2% and 3%). $I_{corr}$ value for blank was 41.3 μA/cm$^2$, whereas $I_{corr}$ value was 7.8 μA/cm$^2$ for 3% rice husk indicating the inhibitive performance of the inhibitor[29].

The influence of calcium nitrite inhibitor to alleviate corrosion on steel rebar embedded in concrete was studied by **Ryu *et al*.,.** The electrochemical impedance spectroscopy results disclosed the effectiveness of $Ca(NO_2)_2$ inhibitor in NaCl. Potentiodynamic polarisation studies exposed the formation of pitting of steel rebar in NaCl medium in the absence of inhibitor. Inhibitor showed a better efficiency of 85.7%[30].

Corrosion resistance performance of *Azadirachta Indica* and Aloevera were investigated by **Lisha *et al*.,** using weight loss measurements. A comparative study was carried out and it has been found that the corrosion inhibition performance of *Azadirachta Indica* was superior than Aloevera extract. It has been found that the rate of corrosion was somewhat high for the conventional concrete. Eco friendly inhibitors exposed better results in conventional concrete containing $Cl^-$ ion. Presence of inhibitors does not alter the hardened nature of the concrete[31].

Barley grass extract was prepared and corrosion inhibition performance on steel in acid medium of 0.1 M HCl has been reported by **Ali *et al*.,** by response surface methodology (RSM). Concentration of the inhibitor was 433-769 ppm, exposure time was 15.4 - 176.8 hours and temperature was 25-45ºC. Kinetic and thermodynamic parameters were calculated. It has been observed that as the exposure time and temperature increased corrosion rate also increased and inhibition efficiency increased with the increase of inhibitor concentration. $\Delta G^o_{ads}$ was negative indicating spontaneous process. The positive value of enthalpy of activation reflected the endothermic process[32].

**Bellal *et al*.,** synthesised a new Schiff base inhibitor 4-hydroxy-3-[1-3-hydroxy-napthalen 2-ylimino-ethyl] 6-methyl-pyran-2-one by condensation method. The efficacy of the inhibitor was examined by EIS and potentiodynamic polarisation studies. The effectiveness of the inhibitor was studied in the hostile environment of 0.5 M NaCl. Inhibition efficiency and activation energy were calculated in order to understand the inhibitive nature of the compound. SEM images were related to the results obtained by EIS measurements. Theoretical calculations were used to determine quantum chemical parameters[33].

**Okeniyi *et al*.,** studied the anti-corrosion behaviour of *Anthocleista djalonensis* admixture on steel embedded in concrete in sulphuric acid medium. The specimens analysed indicated that the corrosion rate highly depends on concentration of the leaf extract as well as the inverse function of noise resistance. Theoretical and experimental approaches were carried out and the results revealed the theoretical efficiency was 96% and experimental was 89.8%. The adsorption process followed Frumkin adsorption isotherm[34].

A comparative study of *Cymbopogan citratus* and $NaNO_2$ in steel in presence of NaCl were monitored by compressive strength improvement - reduction effects and non-destructive electrochemical methods by **Okeniyi *et al.*,.** The results exposed that minimum concentration of 0.0833% of inhibitor was able to impede chloride induced steel in concrete and showed the inhibition efficiency of 99.3%. *Cymbopogan citratus* acted as an excellent corrosion inhibitor in parallel with synthetic inhibitor in saline/marine environment[35].

From the survey of literature, it is evident that limited work has been carried out with natural and synthetic inhibitors to combat rebar corrosion. Hence an attempt has been made to test the validity of two natural and synthetic inhibitors for rebar corrosion.

## 4.3 Experimental materials

### 4.3.1 Inhibitors used for the experiment

Natural inhibitors such as *Cyperus rotundus* and *Rosa damascena* leaves were used for assessing their protection efficiencies on rebar material from corrosion in NaCl.

***Cyperus rotundus***

***Rosa damascena* leaves**

The extracts were prepared as per the procedure discussed in chapter 2. Synthetic inhibitors 5-Amino-1-carbothioamido-4-{[4-N-(4,6-dimethyl-pyrimidin-2-yl)sulfamoyl] phenylazo}pyrazol-5(2H)-one (ACDP) and 6-Amino-5-{[4-N-(4,6-dimethylpyrimidin-2-yl) sulfamoyal]phenylazo}- pyrimidine-2,4-(1H,3H)-dione (ADSD) were utilised to study the efficiency of the inhibitor for mitigating corrosion in steel rebar. These compounds were synthesised based on the procedure in chapter 3. Structure of the synthesised compounds are presented below.

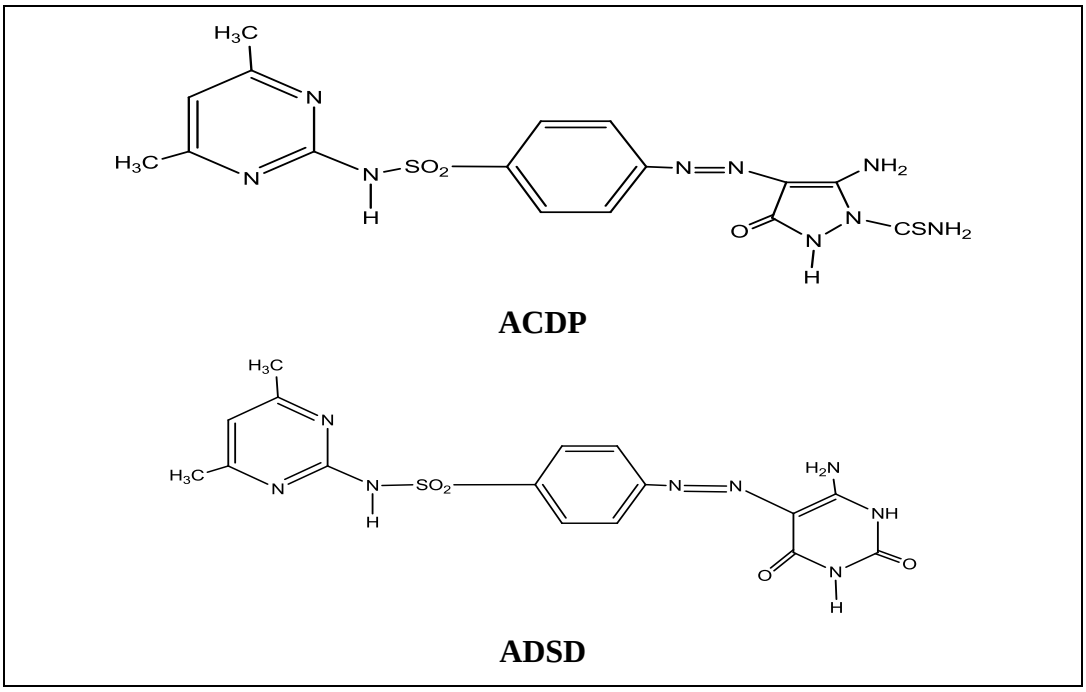


### 4.3.2 Preparation of pore solution and working electrodes

Pore solution of 0.5 M $Ca(OH)_2$, 0.5 M KOH, 0.1 M NaOH was prepared of pH 12.8. The simulated pore solution with chloride ion contains 0.5 M $Ca(OH)_2$, 0.5 M KOH, 0.1 M NaOH, 0.5 M NaCl and it was taken as blank solution. Working electrode used was steel rebar and the specimens obtained from the rebar metal of grade 60 [ASTM A615] of 1 $cm^2$ exposed area. The specimen was descaled by using HCl, drenched with water and dried. The dried specimen was scrapped with a series of emery papers of grade #180 to #1200, finally degreased with acetone and kept for drying.

## 4.4 Experimental methodology

### 4.4.1 Electrochemical techniques

#### 4.4.1.1 Electrochemical impedance spectroscopy (EIS)

Impedance measurements were carried out in the frequency range of 10 kHz to 0.01 Hz with amplitude of 10 mV. From this measurement real (Z') and imaginary parts (Z") were assessed and plots were made. The assessment was carried out in Metro ohm auto lab instrument. The steel bar was immersed in simulated pore solution and impedance measurements were done in inhibited and uninhibited solutions. The protection efficiency was calculated by using the (eqn.1)[36]

$$\text{Protection efficiency } (\%) = \frac{R_{t(in)} - R_{t(bk)}}{R_{t(in)}} x100 \longrightarrow (4.1)$$

where, $R_{t(in)}$ and $R_{t(bk)}$ are charge transfer resistance in the inhibited and uninhibited solutions.

#### 4.4.1.2 Potentiodyamic polarization Techniques

Corrosion kinetic parameters $I_{corr}$, $E_{corr}$, Tafel slopes $b_a$ and $b_c$ were gauged by polarisation techniques and it was carried out for the rebar steel specimens in simulated pore solution with and without inhibitor. The polarisation measurements were carried out in the potential range of -200 mV to +200 mV with respect to the OCP at a scan rate of 1mV/sec. The protection efficiency was calculated by using the relationship in (eqn.2)[37]

$$\text{Protection efficiency } (\%) = \frac{I_{corr(bk)} - I_{corr(in)}}{I_{corr(bk)}} x100 \longrightarrow (4.2)$$

where, $I_{corr(bk)}$ and $I_{corr(in)}$ are denoted as corrosion current densities without and with the accumulation of the inhibitor respectively.

### 4.4.2 Surface morphological studies

#### 4.4.2.1 Fourier transform infrared spectroscopy (FT-IR) analysis

The acid (RDAE) and ethanol (RDEE) extracts were scrutinized for the manifestation of functional groups in the extracts. In order to confirm the adsorption of the inhibitor on the steel rebar, the specimens were immersed in the inhibitors (RDAE, RDEE and ADSD) of optimum concentration containing pore solution for 3 hours at room temperature (303±1K). After the specified time specimens were taken out and air dried. The protective film formed on the specimens were recorded using IR affinity SHIMADZU.

#### 4.4.2.2 Scanning electron microscopy (SEM) and Energy dispersive X-ray spectroscopy (EDS)

SEM images were recorded for steel rebar specimens immersed in pore solution without and with inhibitor for a period of 3 hours. The specimens were removed and washed with water and kept for drying. After drying, the specimens were analysed using SEM coupled with EDS – Carl Zeiss evo18 environmental SEM. The existence of elements on steel rebar was evaluated by EDS detector.

#### 4.4.2.3 Atomic force microscopy (AFM)

The impact of inhibitor on corrosion of steel rebar can be assessed by AFM using NOVA software by multimode scanning probe microscope. It was investigated for the rebar samples after immersion in the uninhibited and inhibited solution for 3 hours.

## 4.5 Results and discussions

### 4.5.1 Electrochemical techniques

#### 4.5.1.1 Electrochemical impedance spectroscopy (EIS)

EIS method represents the performance of the rebar surface in concrete/electrolyte interface[38,39]. In the present study, the pore solution was taken as an electrolyte and it was simulated in order to provide an environment as coastal area and also to study the protection nature of the inhibitor. The electrolyte (pore solution) was simulated with sodium chloride to realize the consequences of chloride ion for corrosion process and also to investigate the ability of the inhibitor. The pH of pore solution was 12.8. The simulated pore solution with chloride was taken as blank and inhibitors were added to this solution at various concentrations of 2, 6, 12 v/v% for natural inhibitors and 1, 3, 5 mM for synthetic inhibitors in order to study their protection efficiency in alkaline medium. The Nyquist plot in the absence of the inhibitor but in the presence of chloride is displayed in **Fig**. **4.1** and datas in **Table 4.1**, which represents the decrease in the loop in the presence of chloride ion as ascribed to the phenomenon that rebar is liable to corrosion suggesting the atrophy of steel in contaminated chloride solution. The oxide films formed may be agitated thus initiating the deterioration of steel rebar due to the rivalry between $OH^-$ and $Cl^-$ ions. With the addition of the inhibitor (natural and synthetic) the value of $R_t$ increases specifying that inhibitor adsorbed on the steel rebar surface also increases resulting in the formation of diffused layer. This layer hinders the metal from the exposure of $Cl^-$ ion and oxygen there by impeding the corrosion process[40,41]. $R_t$ value for blank is 122.4 ohm $cm^2$. At 12 v/v% $R_t$ value for natural inhibitors such as CRAE, CREE, RDAE and RDEE are 577.1, 641.2, 675.6 and 620.4 ohm $cm^2$ and it is presented in **Table 4.2**. At a concentration of 5 mM $R_t$ values for ACDP and ADSD are 680.4 and 621.8 ohm $cm^2$ **(Table 4.3)** suggesting the inhibitory action of the inhibitor. The maximum protection efficiency was 82%. Moreover, higher $R_t$ value decreases the corrosion rate which was apparently due to the inhibitor

utilized which possess higher electron basicity and electron density of hetero atoms which act as the active centres and it is associated with resistance to corrosion which in turn is related to shielding effect due to formation of adherent layer thus shrinking the attack of chloride ions. From the **Figs. 4.2 - 4.4** it is obvious that straight line pattern is obtained rather than semicircles, indicating diffusion controlled mechanism[42]. The results obtained from impedance measurements can be explicated by the equivalent circuit model and it is shown below,

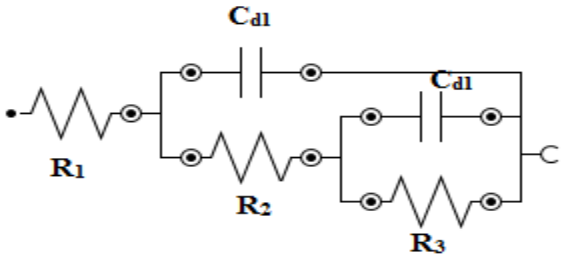


**Fig. e: Equivalent circuit model**

### 4.5.1.2 Potentiodyamic polarization techniques

Polarisation curves of rebar steel sample in the environment of $Ca(OH)_2$ contaminated with NaCl are presented in **Fig. 4.5** and data in **Table 4.4** and for different concentrations of inhibitors are depicted in **Figs. 4.6 - 4.8**. The electrochemical parameters such as $I_{corr}$ (corrosion current), $E_{corr}$ (corrosion potential), $b_a$ (anodic Tafel slope), $b_c$ (cathodic Tafel slope) for natural and synthetic inhibitors are attained by fitting the plots in Tafel regions and are presented in **Tables 4.5 and 4.6**. It is understood from **Tables 4.5 and 4.6** that $I_{corr}$ value of blank is more which is attributed due to the presence of $Cl^-$ ions that attacks the metal surface and enhances corrosion rate significantly. $I_{corr}$ value decreases in presence of inhibitor (CR, RD, ACDP, ADSD) in contrast with blank denoting the formation of passive layer thus blocking the penetration of chloride ion[43-45]. Without the inhibitor NaCl is so hostile resulting in the degradation of steel thus instigating corrosion[46,47]. It can also be implicit that corrosion current density decreases with increase in inhibitor concentration stipulating anodic and cathodic reaction of the rebar steel inhibited by natural as well as synthetic inhibitor. **Figs. 4.6 - 4.8** show a shift in $E_{corr}$ values towards noble direction (positive side) in comparison with blank indicative of adsorption phenomenon by the

inhibitor molecules on the rebar metal. The $I_{corr}$ values for blank, CRAE, CREE, RDAE RDEE, ACDP and ADSD are 410.5, 89.2, 79.8, 75.6, 88.2, 72.6 and 90.5 μA/cm$^2$ with maximum efficiency of 82.3%.

**Effect of $Cl^-$ ions**

The influence of chloride ion in concrete rebars results in corroding the metal to a greater extent. It is well known from literature that the level of chloride ion between 0.4 and 1% (by weight of cement) specifies medium menace of corrosion and produces high threats to corrosion when it reaches above 1%[48]. In order to overcome this issue inhibitor are added to dampen the effect of chloride on concrete. It is obvious from the Nyquist plots and polarisation datas that there is noticeable increase in $R_t$ and substantial decrease in $I_{corr}$ thus proving the nature of the inhibitor to encumber $Cl^-$ ions on the surface of the metal and resulting in the formation of protective film.

### 4.5.2 Adsorption isotherm, surface coverage and protection efficiency

Surface coverage and protection efficiencies were calculated from the polarisation data in **Tables 4.5 and 4.6**. A variation of protection efficiency with the concentration of the inhibitor is depicted in **Figs. 4.9 - 4.11.** Concentration of the inhibitor is plotted against C/θ and it is shown in **Figs. 4.12 - 4.14**. Adsorption is an important phenomenon for inhibition of corrosion which takes place by replacement of water molecules by the inhibitor molecules comprising of hetero atoms[49,50]. Evaluating various adsorption isotherm models, best fit observed for natural and synthetic inhibitor was Langmuir adsorption isotherm and it is given by the eqn (4.3)

$$\frac{C}{\theta} = \frac{1}{K_{ads}} + C \qquad \longrightarrow (4.3)$$

where θ denotes degree of surface coverage, C specifies concentration of the inhibitor and $K_{ads}$ represents adsorption equilibrium constant. It can be viewed from the **Figs. 4.12 - 4.14** that a linear plot is attained with $R^2$ values equal to unity and it is presented in **Tables 4.7 and 4.8**. This proves the formation of monolayer due to active components on the rebar material.

### 4.5.3 Surface morphological studies

#### 4.5.3.1 Fourier transform infrared spectroscopy (FT-IR)

FT-IR spectra are used to validate the presence of functional groups in the plant extracts and also to analyse the adsorption of these extracts on the steel rebar[51]. On comparing the FT-IR spectra of RDAE (extract) and steel rebar immersed in RDAE it is evident that the bands at 3440 $cm^{-1}$ (>OH), 1710 $cm^{-1}$ (>C=O) and 1270 $cm^{-1}$(>C-O), 700 $cm^{-1}$ (>CH) of RDAE has shifted to 3516 $cm^{-1}$, 1733 $cm^{-1}$, 1232 $cm^{-1}$, 702 $cm^{-1}$ in RDAEP respectively. Bands at 3600 $cm^{-1}$(>OH), 1744 $cm^{-1}$ (>C=O), 1260 $cm^{-1}$(>C-O), 650 $cm^{-1}$(>CH) for RDEE has shifted to 3300 $cm^{-1}$, 1749 $cm^{-1}$, 1217 $cm^{-1}$, 665 $cm^{-1}$ for RDEEP (plate). These results specify that there is an interaction of inhibitor with steel rebar hindering corrosion. Results are depicted in **Fig. 4.15**. On analysing the **Fig. 4.16** bands observed for ADSD at 3496 $cm^{-1}$ (-$NH_2$), 3228 $cm^{-1}$ (-NH), 2977 $cm^{-1}$ (-CH), 2160 $cm^{-1}$ (-N=N), 1742 $cm^{-1}$ (-C=O), 1520 $cm^{-1}$(-C=N) are shifted to 3465 $cm^{-1}$, 3276 $cm^{-1}$, 2994 $cm^{-1}$, 2187 $cm^{-1}$, 1743 $cm^{-1}$, 1522 $cm^{-1}$. These results indicate that presence of inhibitor on steel rebar.

#### 4.5.3.2 Scanning electron microscopy (SEM) - Energy dispersive X-ray spectroscopy (EDS)

SEM micrographs of the steel rebar exposed to the environment containing NaCl in the absence and presence of inhibitor are shown in **Fig. 4.17a**. It is evident from **Fig. 4.17a** that steel rebar is damaged and cracks are observed due to the penetration of $Cl^-$ ion indicating that the dissolution of metal takes place without inhibitor[52,53]. The smooth surface without damage observed in **Figs. 4.17b, c** denotes the formation of protective layer of inhibitor on steel rebar averting intrusion of $Cl^-$ ion in turn preventing corrosion. Visual examination of **Fig. 4.17d** proves that adsorbed inhibitor film act as protective layer thus blocking the metal from intrusion of $Cl^-$ ion promoting a shielding effect and mitigating corrosion. **Fig. 4.17a** indicates EDS results for steel rebar in simulated pore solution without inhibitor. In the absence of inhibitor there is an existence of chloride ion. The EDS spectra **(Figs. 4.17b, c and d)** in presence of inhibitor divulges the presence of carbon atoms denoting the adsorption of the inhibitor on the rebar surface. Elemental composition is presented in **Table 4.9**.

### 4.5.3.3 Atomic force microscopy (AFM)

AFM is a useful technique to study the roughness of the metal surface and also to analyse the generation and development of corrosion products[54]. A 2D and 3D view of AFM images of the steel rebar with and without the addition of inhibitor in simulated pore solution are depicted in **Fig. 4.18**. It can be viewed from **Fig. 4.18a** that the surface was damaged in the absence of inhibitor resulting in the dissolution of the steel rebar which may be due to the attack of $Cl^-$ ion. **Figs. 4.18b, c and d** shows reduced roughness in presence of inhibitor indicating the formation of protective layer thus hindering the $Cl^-$ ion reaching the metal surface[55]. Average roughness calculated for blank solution is 79.56 nm, whereas the values obtained for the inhibited steel rebar RDAE, RDEE and ADSD are 23.07 nm, 38.06 nm and 32.14 nm. It is obvious from these data that reduction in average roughness impute that steel rebar is protected from corrosion in presence of inhibitor.

## 4.6 Mechanism for inhibition

The pore solution in concrete act as an electrolyte. Chloride ions and carbon dioxide may intrude into the concrete and affect the reinforced steel rebar and corrosion process gets instigated[56]. In reinforced steel there are two different regions anode and cathode. The iron is transformed to ferrous ions and electrons; it migrates from anode to cathode. Ferric hydroxide which is rust occupies a greater volume resulting in generation of fissures, decrease in adhesion, and detachment of concrete thus tumbling life span of the metal. The influence of chloride ions results in the undermining of the passivating layer. The chloride ion reacts with Fe and $OH^-$ to form iron hydroxide. The accessible free chloride continues to react. In carbonation process $CO_2$ infiltrates into the concrete through dispersion and reacts with water to produce carbonic acid. In order to overcome this issue, inhibitors (natural and synthetic) are used which has a tendency to bond with the metal either physical (or) chemical adsorption thus impeding the anodic and cathodic reactions and form a protective layer and retard corrosion. Inhibitors (natural and synthetic) used contain heteroatoms such as O, N, S and aromatic rings which may collectively intricate in having additional sites and form a protective layer thus hindering the depolarising agents ($O_2$, $Cl^-$) into interaction with reinforced steel surface thus impeding the corrosion process. It is well known that that the affinity of $Cl^-$ ion towards the steel is more because of

electronegativity of it. Chloride ion easily reacts with iron producing iron chloride but inhibitor (natural and synthetic) deactivates the reaction. The predominant components such as 4-hydroxy chalcone, in natural inhibitors contains OH groups which have a tendency to form a coordinate bond with iron ensuing in the creation of complexes with metal. Schematic representation of mechanism of rebar corrosion in presence of natural inhibitor is shown in **Fig. 4.19a**. The formed complexes retard micro anodes produced on the surface of the metal thus impeding the metal dissolution. The electro active nitrogen, oxygen atoms and electron rich aromatic ring of the inhibitors (CR and RD) lead to adsorption. A detailed view of mechanism in **Fig. 4.19b** suggests that large area of the molecule (ACDP and ADSD) with heteroatoms have a greater capability to spread throughout the metal surface and also have a tendency to adhere on the surface thus hindering the corrosion. Added inhibitor has an ability to suppress the attack of $Cl^-$ ion on rebar steel. The guarding effect of both the inhibitors are due to existence of organic moieties which may result in blocking the flow of electrons on metal/concrete boundary acting as a barrier to these hostile ions and protect the metal from corrosion.

### 4.7 Conclusions

Based on the above results subsequent conclusions can be drawn

- Inhibitor proficiently alleviated the corrosion in steel rebar. The aggressiveness of $Cl^-$ is curbed in presence of natural and synthetic inhibitors.
- Protection efficiency of the inhibitor proves the nobility of the inhibitor.
- Impedance studies unveiled a guarding effect of the inhibitor against corrosion taking place in rebar material which is proved by an increase of $R_t$ with concentration.
- Steel rebar exposed to different concentrations of the inhibitor containing simulated pore solution contaminated with $Cl^-$ ion displayed adsorption phenomena on steel rebar following Langmuir adsorption isotherm ascertaining monolayer of adsorption of the inhibitor.
- SEM and AFM images proved the enhanced protective layer in presence of inhibitor.

## 4.8 References


1. H. Gerengi, Y. Kocak, A. Jazdzewska, H. Kurtay, H. Durgun, Constr. Build. Mater., **49** (2013) 471.
2. X. Shi, N. Xie, K. Fortune, J. Gong, Constr. Build. Mater., **30** (2012) 125.
3. http://www.materialsperformance.com/articles/material-selection-design/2015/12/ corrosion -effects-on-the durability-of-reinforced-concrete-structures.
4. https://www.markhamglobal.com/concrete-cancer-silent-killer.
5. https://the constructor.org/concrete/corrosion-steel-reiforcement-concrete/6179.
6. U.M. Angst, Mater. Struct., (2018) http://doi.org/10.1617/s11527-017-1131-6.
7. M.M. Mennucci, E.P. Banczek, P.R.P. Rodrigues, Cem. Concr. Compos., **31** (2009) 418.
8. X. Zhu, G. Zi, Cao and X. Cheng, Constr. Build. Mater., **110 (**2016) 369.
9. T.A. Soylev, M.G. Richardson, Constr. Build. Mater., **22** (2008) 609.
10. Materials and methods for corrosion control of reinforced and pre stressed concrete structures in new construction (book), US department of transportation publication no 00081, 2000.
11. S.M. Trepanier, B. Hope, C.M. Hansson, Cem. Concr. Res., **3** (2001) 713.
12. H. Zheng, W. Li, F. Ma, Q. Kong, Cem. Concr. Res., **55** (2014) 102.
13. M.G.L. Annamalai, G. Maheswaran, R. Yuvaraja, R. Jayakodi, Int. J. Chemtech Res., **8** (2015) 178.
14. M.A. Quraishi, D. Nayak, V. Kumar, J. Steel Struct Constr., **3** (2017) 1.
15. A. Charis, J. Appl. Mech. Eng., **1** (2012) 1.
16. https://civildigital.com/effects-corrosion-reinforcement-signs-preventive-measures.
17. G. Batis, P. Pantazopoulou, A. Routoulas, Cem. Concr Compos., **25** (2003) 371.
18. H. Saricimen, M. Mohammed, A. Quddus, M.S. Shameem, Barry, Cem. Concr Compos., **24** (2002) 89.
19. S. Har Kumer, S. Karthikeyan, J. Mater. Enviro. Sci., **3** (2012) 925.

20. M.A. Deyab, M.M. Osman, A.E. Elkholy, F. El-TaibHeakal, RSC Advances., **7** (2017) 45241.
21. D.G. Eyu, H. Esah, C. Chukwuekezie, J. Idris, I. Mohammad, ARPN J. Eng. Appl. Sci., **8** (2013) 326.
22. S.A. Asipita, M. Ismail, M.Z. Abd Majid, Z. Abdul Majid, C. Abdullah, J. Mirza, J. Clean. Prod., **67** (2014) 139.
23. L. Feng, X. Cui, J. Wang, H. Yang, F. Wang, Adv. Mater. Res., **1090** (2015) 69.
24. A.S. Mahdi, S.K. Rahem, M.J. Nehab, IJARET., **6** (2015) 33.
25. H.S. Lee, H.S. Ryu, W.J. Park, A. Ismail, Materials., **8** (2015) 251.
26. I. Cherif, L. Dhouibi, E. Triki, J. Mater. Environ. Sci., **6** (2015) 1364.
27. J.O. Okeniyi, C.A. Loto, A.P.I. Popoola, Solid. State. Phenom., **227** (2015) 281.
28. J. O. Okeniyi, C.A. Loto, A.P.I. Popoola., Metals **6** (2016) 1.
29. S.A. Abdulsada, A.I.A. Mosawi, A.A.A. Hadi, Bioprocess. Engg., **3** (2017) 81.
30. H.W. Ryu, J.K. Singh, H.S. Lee, W.J. Park, Adv. Mater. Sci., **2017** (2017) 1.
31. C. Lisha, M. Rajalingam, G. Sunilaa, IJESIRD., **3** (2017) 687.
32. A. Ali, S. Falih, N. Yousif, R. Rezgar, I. Kamal, Amer. J. Env. Engg., **7** (2017) 73.
33. Y. Bellal, S. Keraghel, F. Benghanem, T. Linda, G. Sigrcik, B. Riadh, A. Ourari, Int. J. Electrochem. Sci., **13** (2018) 7218.
34. J.O. Okeniyi, A.P.I. Popoola, ARPN J. Eng. Appl. Sci., **13** (2018) 1553.
35. J.O. Okeniyi, A.P. I. Popoola, O.E. Toyin, Int. J. Corros., **2018** (2018) 1.
36. P. Sounthari, A. Kiruthika, J. Saranya, K. Parameswari, S. Chitra, Ecotoxicol. Environ Saf., **134** (2016) 319.
37. S. Saranya, M. Sowmiya, P. Sounthari, K. Parameswari, S. Chitra, K. Senthilkumar, J. Mol. Liq., **216** (2016) 42.
38. W. Medford, Transp. Res. Rec., **1795** (2014) 62.
39. H. Ryu, J.K. Singh, H.M. Yang, H. Lee, M.A. Ismail, Constr. Build. Mater., **114** (2016) 223.

40. V. Saraswathy, H.W. Song, Build. Environ., **42** (2007) 464.

41. Y. Zhou, Y. Zuoz, J. Electrochem. Soc., **162** (2015) 47.

42. C. Nusrath Unnisa, G. Nirmala Devi, V. Hemapriya, S. Chitra, I.M. Chung, S.H. Kim, M. Prabakaran, Constr. Build. Mater., **165** (2018) 866.

43. B. Youcef, K. Saida, B. Fatiha, T. Linda, S. Gokmen, B. Bourzami, O. Ali, Int. J. Electrochem. Sci., **13** (2018) 7218.

44. M. Abulrasoul Salih, IJARET., **5** (2014) 30.

45. E. Hernandez, P.F.J. Cano Barrita, F.M. Leon-Martinez, A.T. Acosta, Anti- Corros. Methods Mater., **64** (2017) 529.

46. N. Anusuya, J. Saranya, P. Sounthari, A. Zarrouk, S. Chitra, J. Mol. Liq., **225** (2017) 406.

47. M. Yadav, S. Kumar, Surf. Interface. Anal., **46** (2014) 129.

48. S.K. Verma, S.S. Bhadauria, S. Akhtar, Front. Struct. Civ. Eng., **7** (2013) 379.

49. S.A. Fouda, A.A.E Hossiany, M.H. Ramadan, Zastita Materijala., **58** (2017) 541.

50. Z.V.P. Murthy, K. Vijayargavan, Green chem. Lett. Rev., **7** (2014) 209.

51. S.M. Trepanier, B. Hope, C.M. Hansson, Cem. Concr. Res., **3** (2001) 713.

52. M. Hassoune, A. Bezzar, L. Sail, F. Ghomari, J. Adhes. Sci. Technol., (2017) https://doi.org/10.1080/01694243.2017.1341190.

53. L. Li, A.A. Saguess, Corrosion., **57** (2001) 19.

54. P. Sakunthala, P. Vivekanathan, M. Gopiraman, N. Sulochana, A.R. Vincent, J. Surfact. Deterg., **16** (2013) 251.

55. A.M. Masmoudi, J. Bouaziz, Adv. Mater. Sci. Eng., **2016** (2016) 1.

56. H. Zheng, J.G. Dai, C.S. Poon, W. Li, Cement. Concrete. Res., **108** (2018) 46.

**Table 4.1: AC-impedance parameters for the pore solution in the absence and presence of chloride**

| Solution | $R_t$ (ohm $cm^2$) | $C_{dl}$ (µF/$cm^2$) |
|---|---|---|
| **Pore solution in the absence of $Cl^-$** | 234.2 | 19.6 |
| **Pore solution in the presence of $Cl^-$** | 122.4 | 25.2 |

**Table 4.2: AC-impedance parameters for corrosion in rebar in the presence of selected concentrations of acid and ethanol extracts of CR and RD**

| Name of the inhibitor | Conc. (v/v%) | $R_t$ (ohm $cm^2$) | $C_{dl}$ (µF/$cm^2$) | IE(%) |
|---|---|---|---|---|
| **Pore solution in the presence of $Cl^-$** | - | 122.4 | 25.2 | - |
| **CRAE** | 2 | 300.2 | 13.1 | 59.2 |
| | 6 | 477.4 | 11.3 | 74.4 |
| | 12 | 577.1 | 10.7 | 78.8 |
| **CREE** | 2 | 279.7 | 13.7 | 56.2 |
| | 6 | 471.6 | 11.2 | 74.0 |
| | 12 | 641.2 | 9.6 | 80.9 |
| **RDAE** | 2 | 249.5 | 15.4 | 50.9 |
| | 6 | 525.1 | 11.6 | 76.7 |
| | 12 | 675.6 | 9.1 | 81.9 |
| **RDEE** | 2 | 220.6 | 14.7 | 44.5 |
| | 6 | 420.1 | 11.5 | 70.8 |
| | 12 | 620.4 | 9.4 | 80.2 |

**Table 4.3: AC-impedance parameters for corrosion in rebar in the presence of selected concentrations of synthetic inhibitors ACDP and ADSD**

| Name of the inhibitor | Conc. (mM) | $R_t$ (ohm $cm^2$) | $C_{dl}$ ($\mu F/cm^2$) | IE (%) |
|---|---|---|---|---|
| **Pore solution in the presence of $Cl^-$** | - | 122.4 | 25.2 | - |
| **ACDP** | 1 | 267.4 | 14.1 | 54.2 |
| | 3 | 467.1 | 11.4 | 73.8 |
| | 5 | 680.4 | 8.9 | 82.0 |
| **ADSD** | 1 | 260.1 | 14.2 | 52.9 |
| | 3 | 445.2 | 11.9 | 72.5 |
| | 5 | 621.8 | 9.4 | 80.3 |

**Table 4.4: Potentiodynamic polarization parameters for the pore solution in the absence and presence of chloride**

| Solution | Tafel slopes (mV/dec) | | $-E_{corr}$ (mV) | $I_{corr}$ ($\mu A/cm^2$) |
|---|---|---|---|---|
| | $b_a$ | $b_c$ | | |
| **Pore solution in the absence of $Cl^-$** | 158 | 44 | 757 | 363.2 |
| **Pore solution in the presence of $Cl^-$** | 190 | 61 | 680.8 | 410.5 |

**Table 4.5: Potentiodynamic polarization parameters for corrosion in rebar in the presence of selected concentrations of acid and ethanol extracts of CR and RD**

| Name of the inhibitor | Conc. (v/v%) | Tafel slopes (mV/dec) | | -$E_{corr}$ (mV) | $I_{corr}$ ($\mu A/cm^2$) | IE (%) | Surface coverage (C/θ) |
|---|---|---|---|---|---|---|---|
| | | $b_a$ | $b_c$ | | | | |
| **Pore solution in the presence of $Cl^-$** | - | 190 | 61 | 680.8 | 410.5 | - | - |
| **CRAE** | 2 | 258 | 59 | 670.1 | 202.1 | 50.8 | 3.937 |
| | 6 | 271 | 67 | 637.6 | 126.2 | 69.3 | 8.658 |
| | 12 | 297 | 84 | 633.1 | 89.2 | 78.3 | 15.326 |
| **CREE** | 2 | 235 | 68 | 598.4 | 198 | 51.8 | 3.861 |
| | 6 | 118 | 51 | 584.5 | 108.6 | 73.5 | 8.163 |
| | 12 | 110 | 45 | 598.6 | 79.8 | 80.6 | 14.888 |
| **RDAE** | 2 | 244 | 88 | 597.9 | 210 | 48.8 | 4.098 |
| | 6 | 242 | 97 | 590.7 | 110.5 | 73.1 | 8.207 |
| | 12 | 305 | 109 | 592.7 | 75.6 | 81.6 | 14.705 |
| **RDEE** | 2 | 115 | 37 | 662.5 | 235.5 | 42.6 | 4.695 |
| | 6 | 255 | 63 | 634.9 | 125.6 | 69.4 | 8.645 |
| | 12 | 313 | 66 | 628.4 | 88.2 | 78.5 | 15.286 |

**Table 4.6: Potentiodynamic polarization parameters for corrosion in rebar in the presence of selected concentrations of ACDP and ADSD**

| Name of the inhibitor | Conc. (mM) | Tafel slopes (mV/dec) | | -$E_{corr}$ (mV) | $I_{corr}$ ($\mu A/cm^2$) | IE (%) | Surface coverage (C/θ) |
|---|---|---|---|---|---|---|---|
| | | $b_a$ | $b_c$ | | | | |
| **Pore solution in the presence of $Cl^-$** | - | 190 | 61 | 680.8 | 410.5 | - | - |
| **ACDP** | 1 | 157 | 29 | 573.2 | 201.8 | 50.8 | 1.97 |
| | 3 | 117 | 33 | 554.6 | 110.7 | 73.0 | 4.11 |
| | 5 | 108 | 57 | 537.6 | 72.6 | 82.3 | 6.08 |
| **ADSD** | 1 | 107 | 31 | 589.8 | 210.2 | 48.8 | 2.05 |
| | 3 | 113 | 42 | 580.2 | 112.8 | 72.5 | 4.14 |
| | 5 | 143 | 57 | 575.9 | 90.5 | 78.0 | 6.41 |

**Table 4.7: Langmuir adsorption parameters of acid and ethanol extracts of CR and RD on rebar material**

| Inhibitor | $R^2$ | Slope | K mol $lt^{-1}$ |
|---|---|---|---|
| **CRAE** | 0.9997 | 1.08 | 178 |
| **CREE** | 0.9991 | 1.09 | 121 |
| **RDAE** | 0.9996 | 1.06 | 236 |
| **RDEE** | 0.9988 | 1.07 | 191 |

**Table 4.8: Langmuir adsorption parameters of ACDP and ADSD**

| Inhibitor | $R^2$ | Slope | K mol $lt^{-1}$ |
|---|---|---|---|
| **ACDP** | 0.9998 | 1.09 | 164 |
| **ADSD** | 0.9988 | 1.06 | 176 |

**Table 4.9: Composition of elements in uninhibited and inhibited metal specimen**

| Sample | Fe | C | O | Cl | Na |
|---|---|---|---|---|---|
| **Blank** | 74.08 | 1.96 | 15.26 | 8.50 | 0.2 |
| **RDAE** | 67.50 | 16.72 | 14.38 | 1.22 | 0.18 |
| **RDEE** | 67.80 | 15.96 | 14.59 | 1.48 | 0.17 |
| **ADSD** | 67.68 | 16.54 | 14.34 | 1.24 | 0.2 |

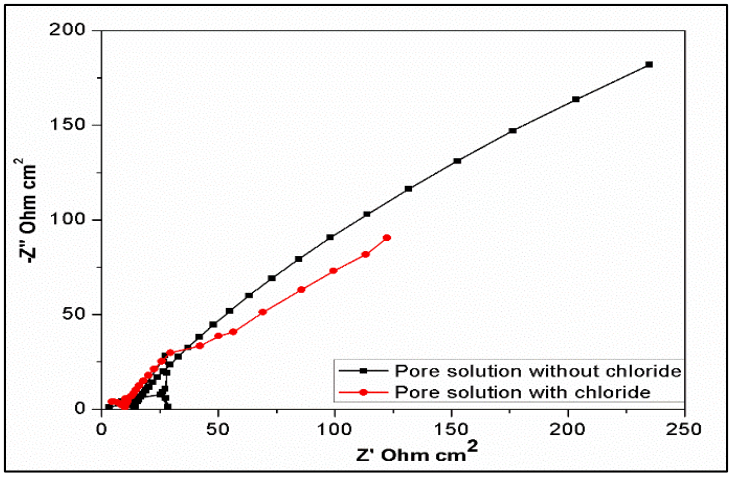


**Fig. 4.1: Impedance spectra of pore solution in the presence and absence of chloride**

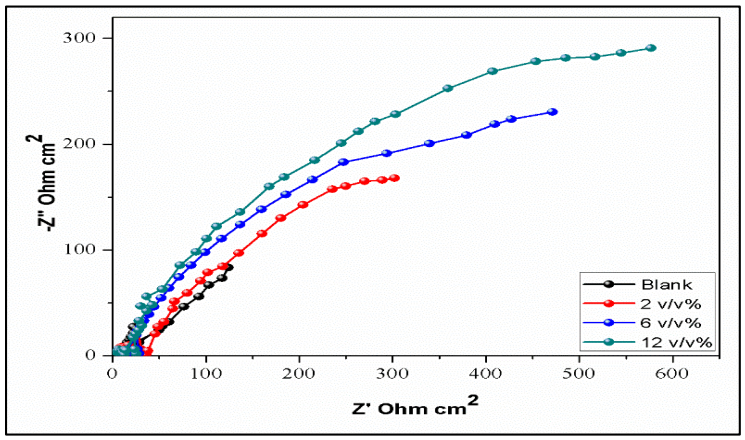


**Fig. 4.2(a): Nyquist plot of various concentrations of CRAE for the corrosion of steel rebar**

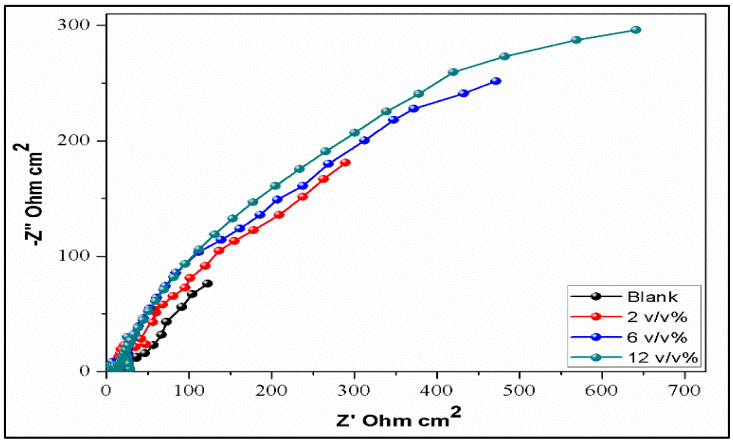


**Fig. 4.2(b): Nyquist plot of various concentrations of CREE for the corrosion of steel rebar**

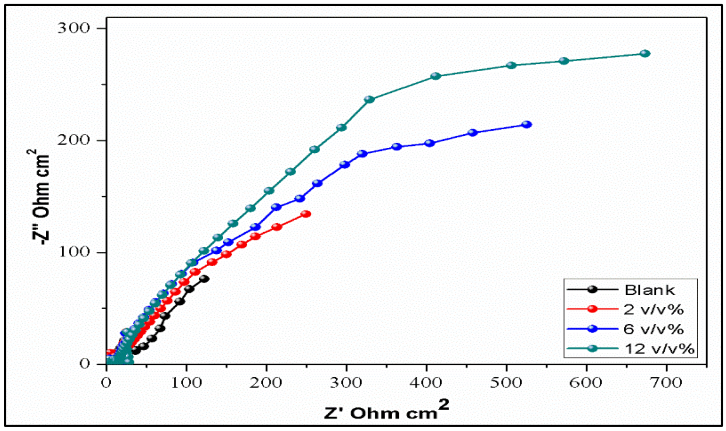


**Fig. 4.3(a): Nyquist plot of various concentrations of RDAE for the corrosion of steel rebar**

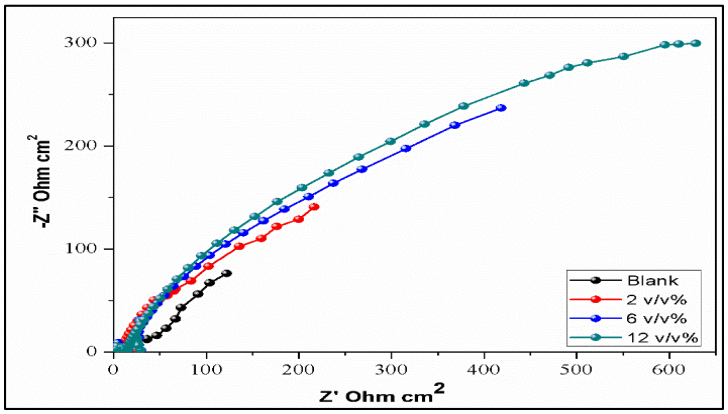


**Fig. 4.3(b): Nyquist plot of various concentrations of RDEE for the corrosion of steel rebar**

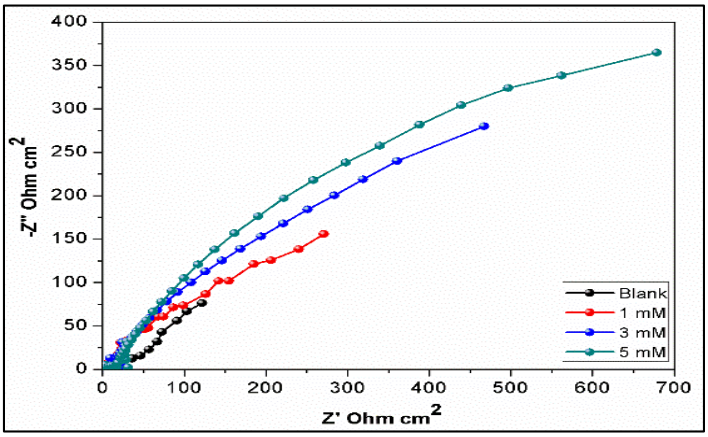


**Fig. 4.4(a): Nyquist plot of various concentrations of ACDP for the corrosion of steel rebar**

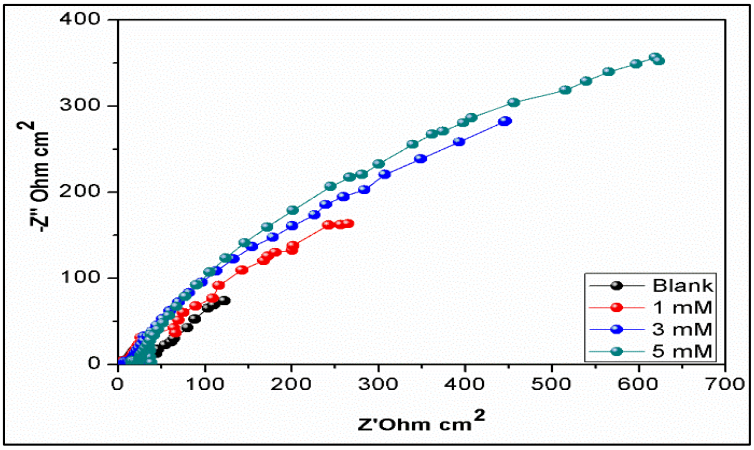


**Fig. 4.4(b): Nyquist plot of various concentrations of ADSD for the corrosion of steel rebar**

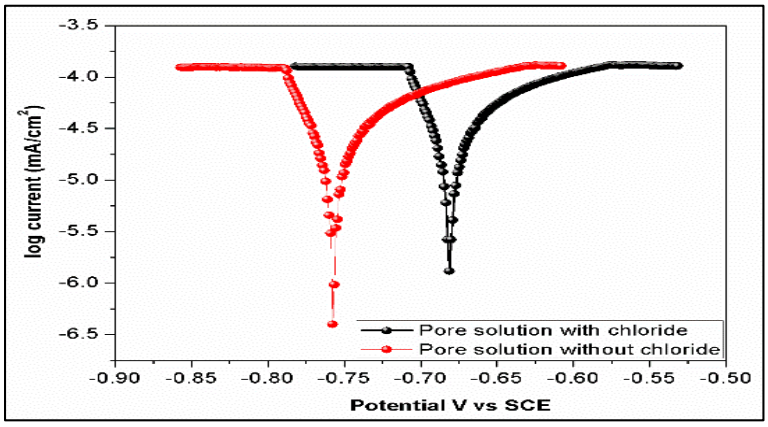


**Fig. 4.5: Tafel polarisation plots of pore solution in the absence and presence of chloride**

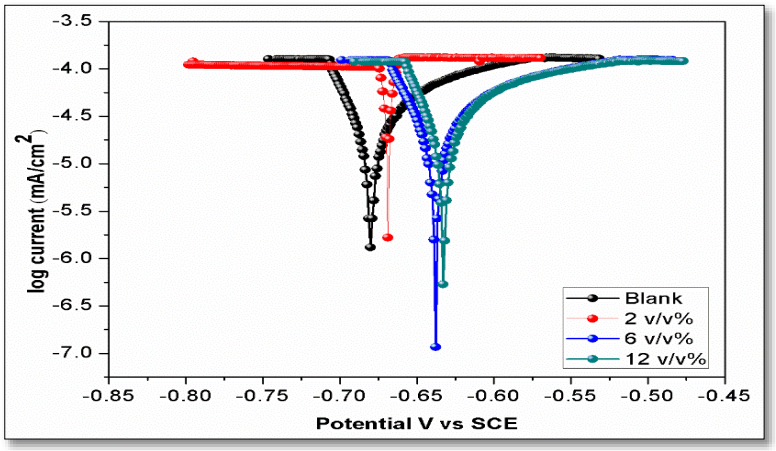


**Fig. 4.6(a): Tafel polarisation plots of various concentrations of CRAE**

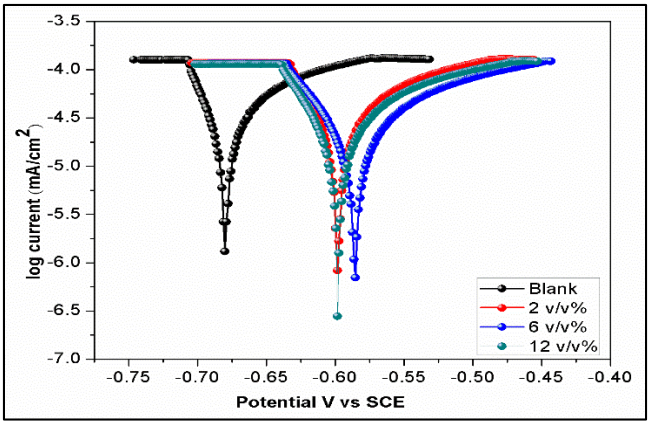


**Fig. 4.6(b): Tafel polarisation plots of various concentrations of CREE for corrosion on steel rebar**

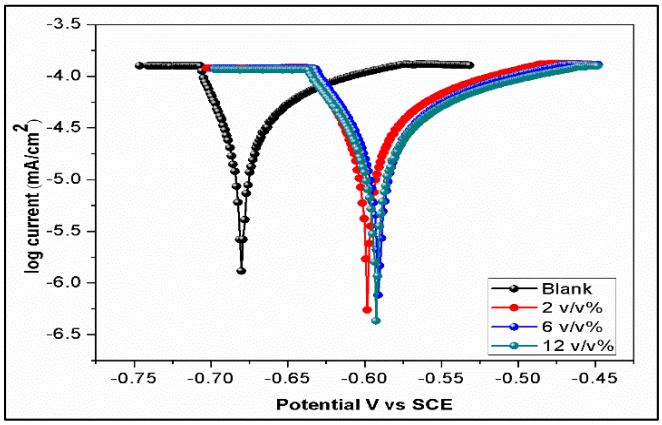


**Fig. 4.7(a): Tafel polarisation plots of various concentrations of RDAE for corrosion on steel rebar**

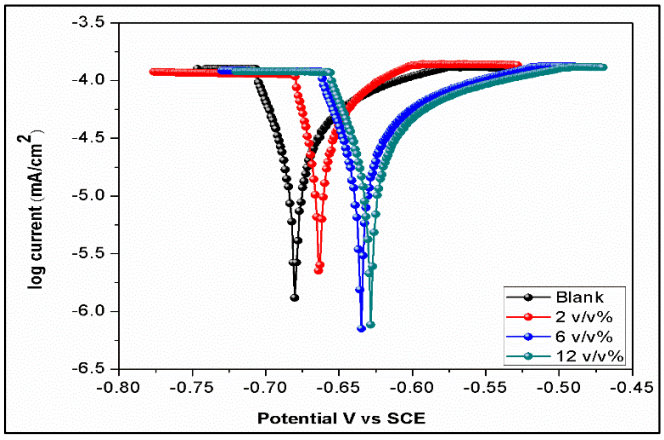


**Fig. 4.7(b): Tafel polarisation plots of various concentrations of RDEE for corrosion on steel rebar**

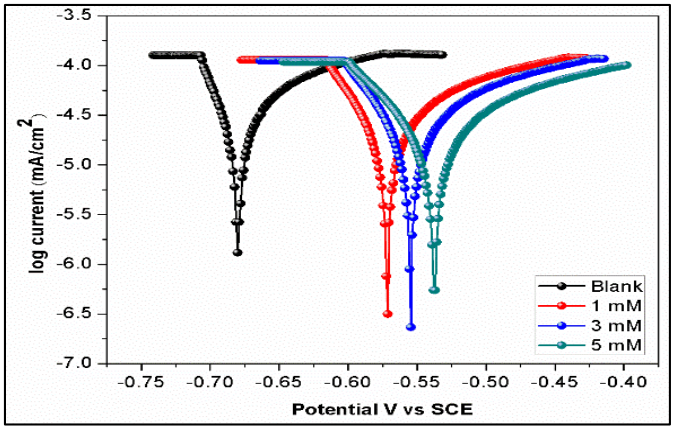


**Fig. 4.8(a): Tafel polarisation plots of various concentrations of ACDP corrosion on steel rebar**

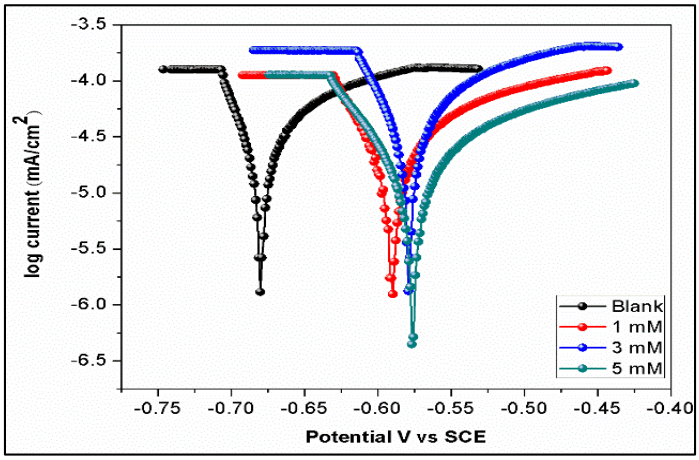


**Fig. 4.8(b): Tafel polarisation plots of various concentrations of ADSD corrosion on steel rebar**

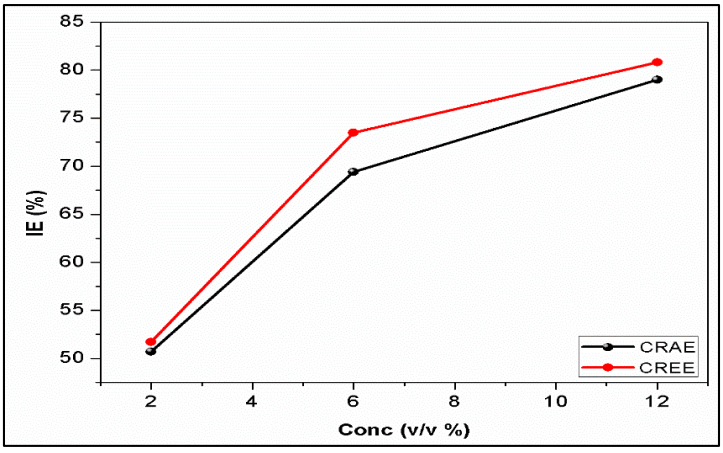


**Fig. 4.9: Plot of Concentration vs. IE (%) for CRAE and CREE**

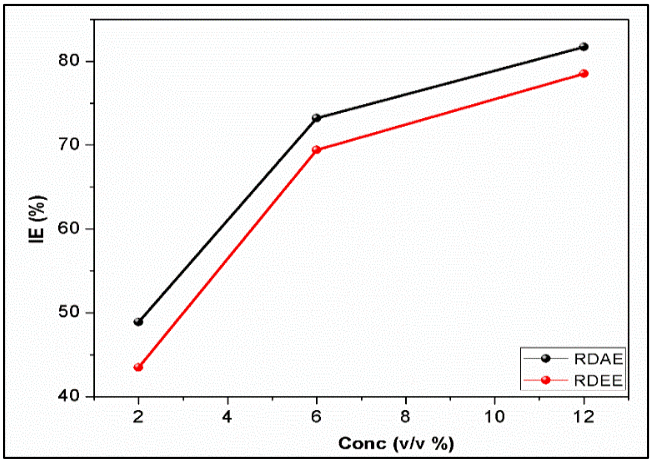


**Fig. 4.10: Plot of Concentration vs. IE (%) for RDAE and RDEE**

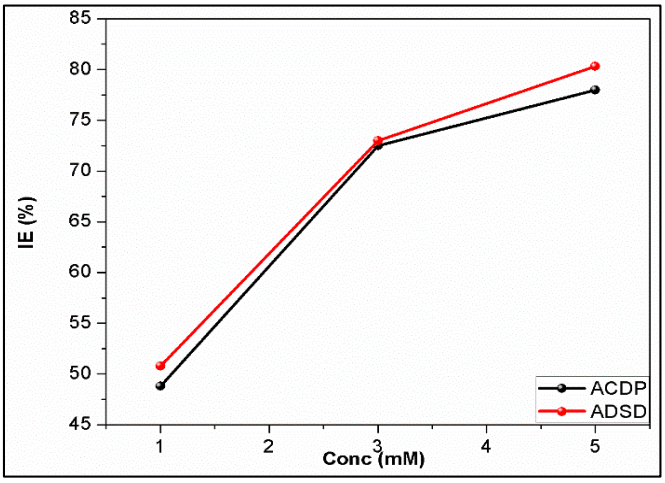


**Fig. 4.11: Plot of Concentration vs. IE (%) for ACDP and ADSD**

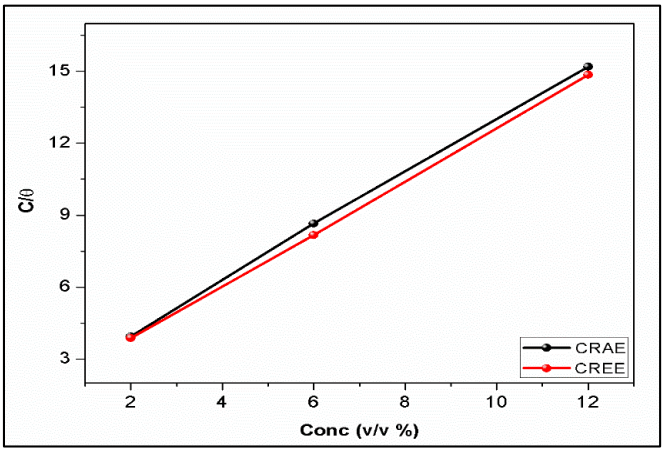


**Fig. 4.12: Langmuir plot for rebar in presence of different concentrations of CRAE and CREE**

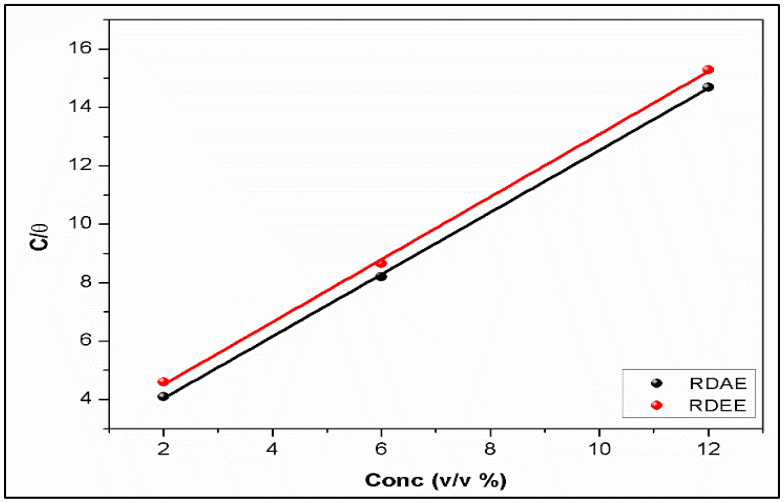


**Fig. 4.13: Langmuir plot for rebar in presence of different concentrations of RDAE and RDEE**

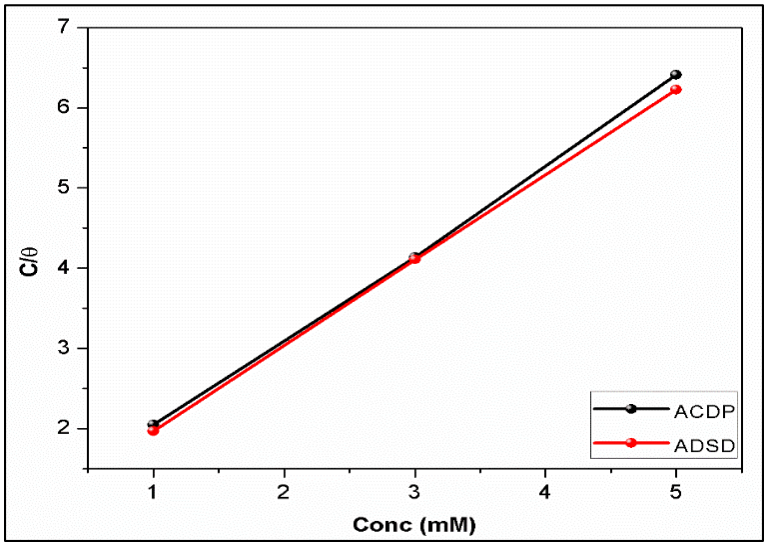


**Fig. 4.14: Langmuir plot for rebar in presence of different concentrations of ACDP and ADSD**

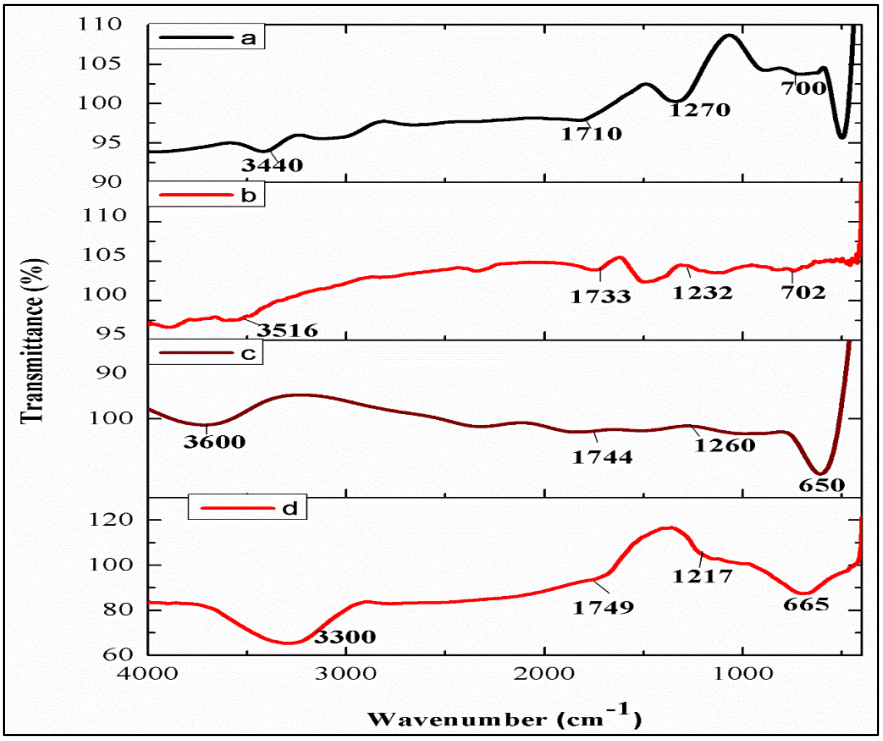


**Fig. 4.15: IR spectra of inhibitor (a) RDAE (c) RDEE and inhibitor adsorbed on steel rebar in simulated pore solution (b) RDAEP (d) RDEEP**

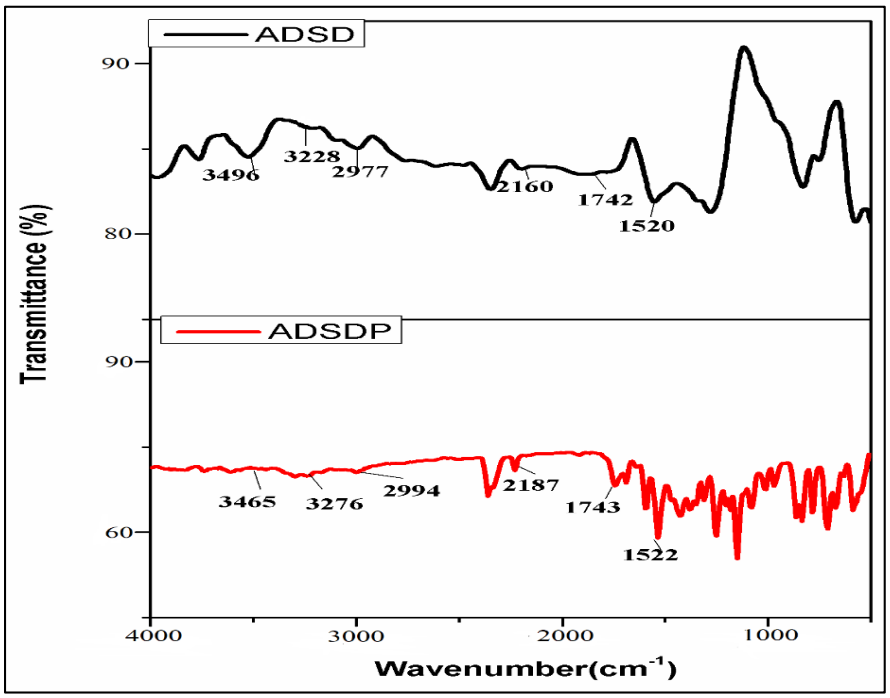


**Fig. 4.16: IR spectra of ADSD inhibitor and ADSDP adsorbed on steel rebar in simulated pore solution**

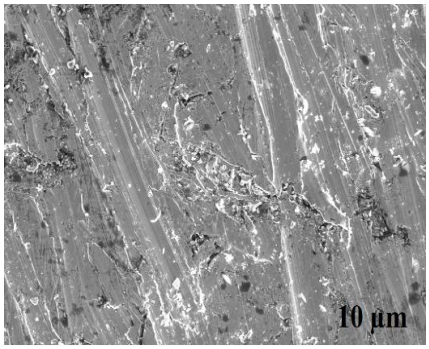


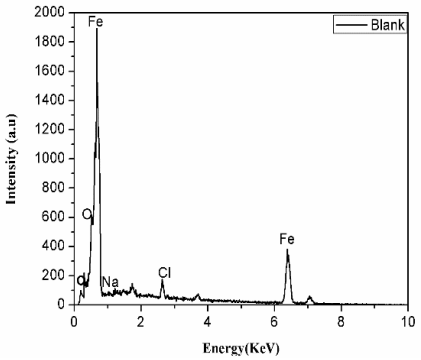


**(a)**

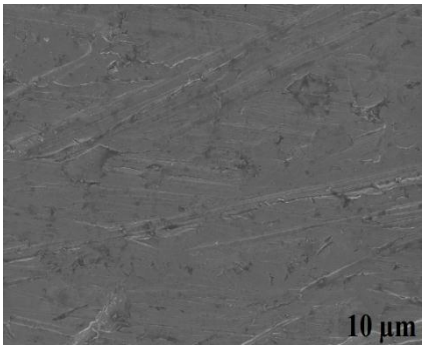


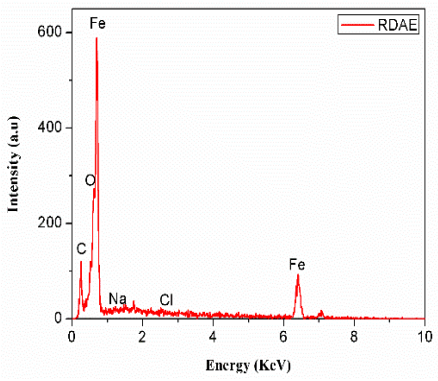


**(b)**

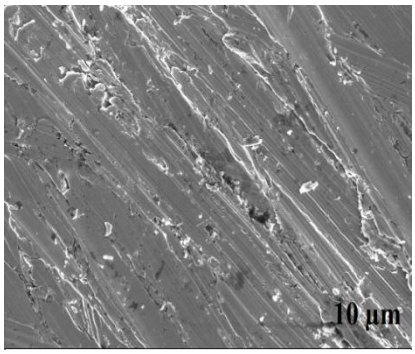


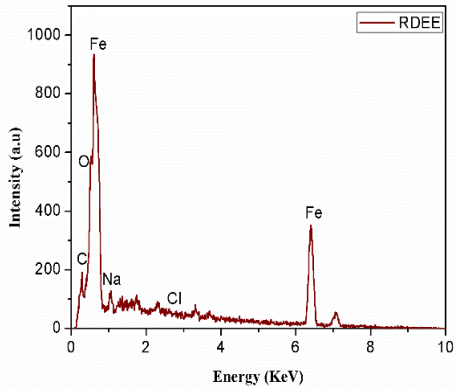


**(c)**

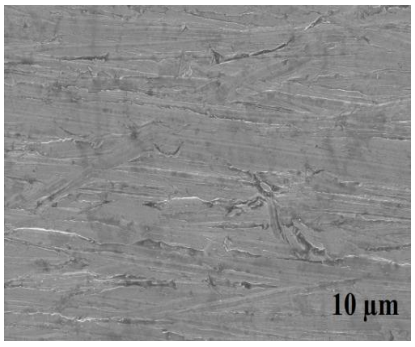


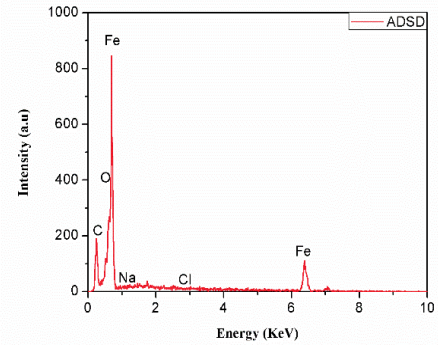


**(d)**

**Fig. 4.17: SEM-EDS spectra of steel rebar (a) without inhibitor (b) RDAE (c) RDEE (d) ADSD**

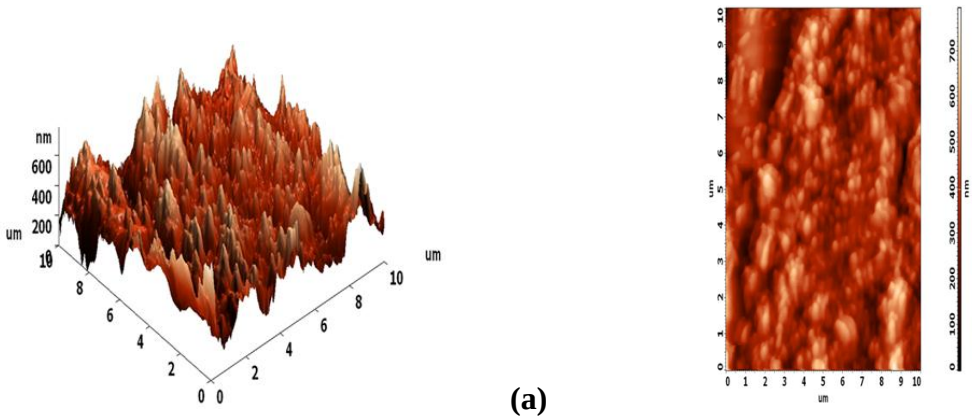
nm
600
400
200
um
10
8
6
4
2
0
0
2
4
6
8
10
um
um
0 1 2 3 4 5 6 7 8 9 10
um
0
100
200
300
400
500
600
700
nm

**(a)**

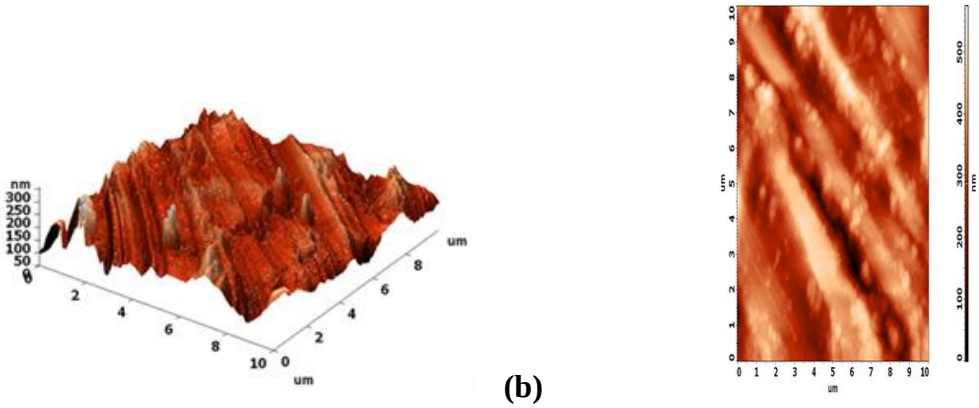
nm
300
250
200
150
100
50
0
2
4
6
8
10
0
2
4
6
8
um
um
0 1 2 3 4 5 6 7 8 9 10
um
0
100
200
300
400
500
nm

**(b)**

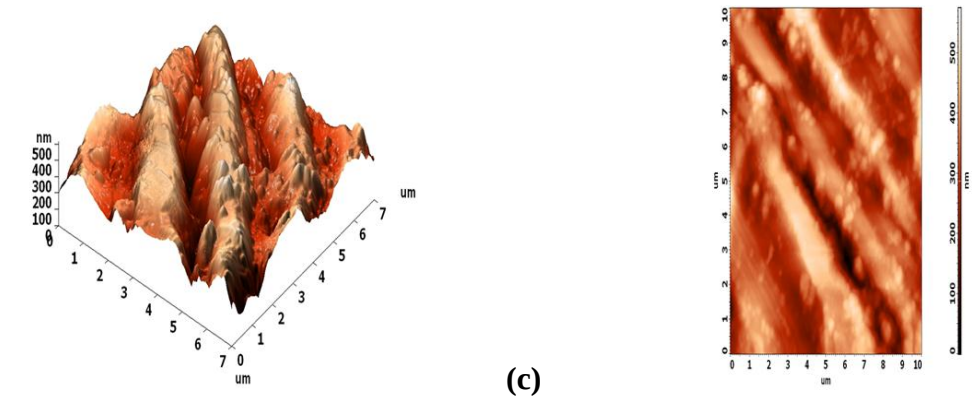
nm
500
400
300
200
100
0
1
2
3
4
5
6
7
0
1
2
3
4
5
6
7
um
um
0 1 2 3 4 5 6 7 8 9 10
um
0
100
200
300
400
500
nm

**(c)**

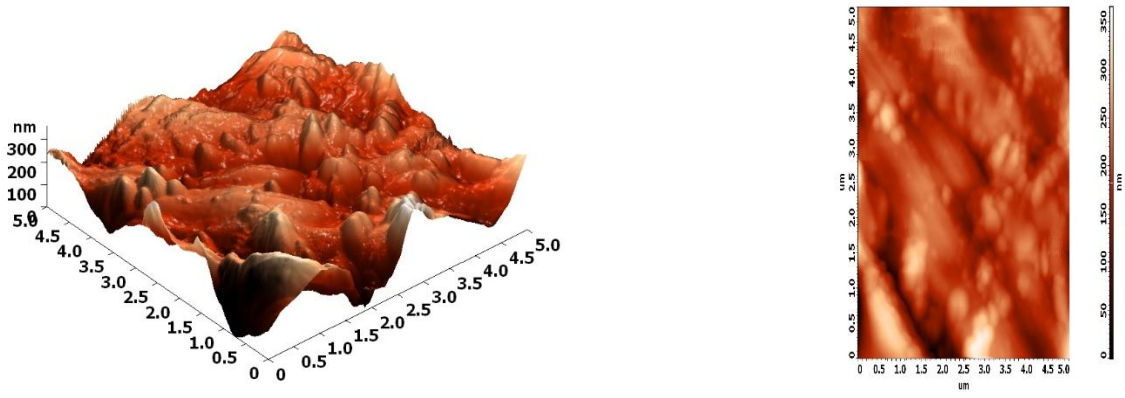


**(d)**

**Fig. 4.18: 3D and 2D AFM images of (a) without inhibitor (b) RDAE (c) RDEE (d) ADSD**

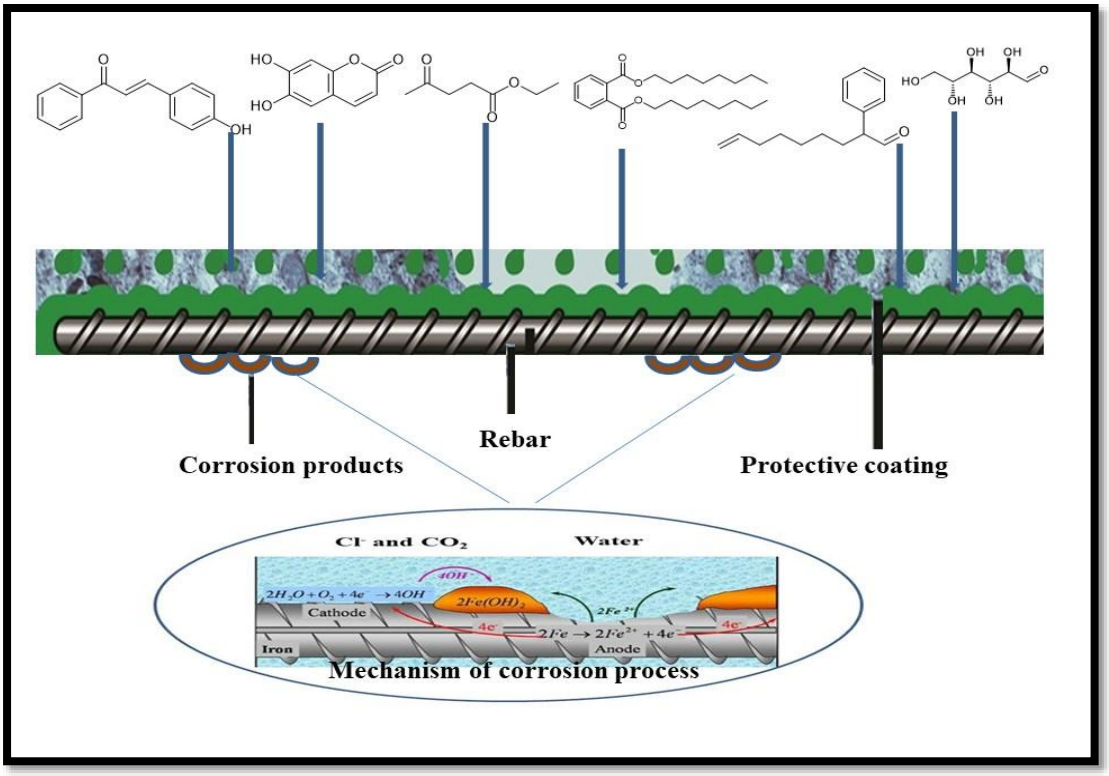


**Fig. 4.19(a): Schematic representation of mechanism of rebar corrosion in presence of natural inhibitors**

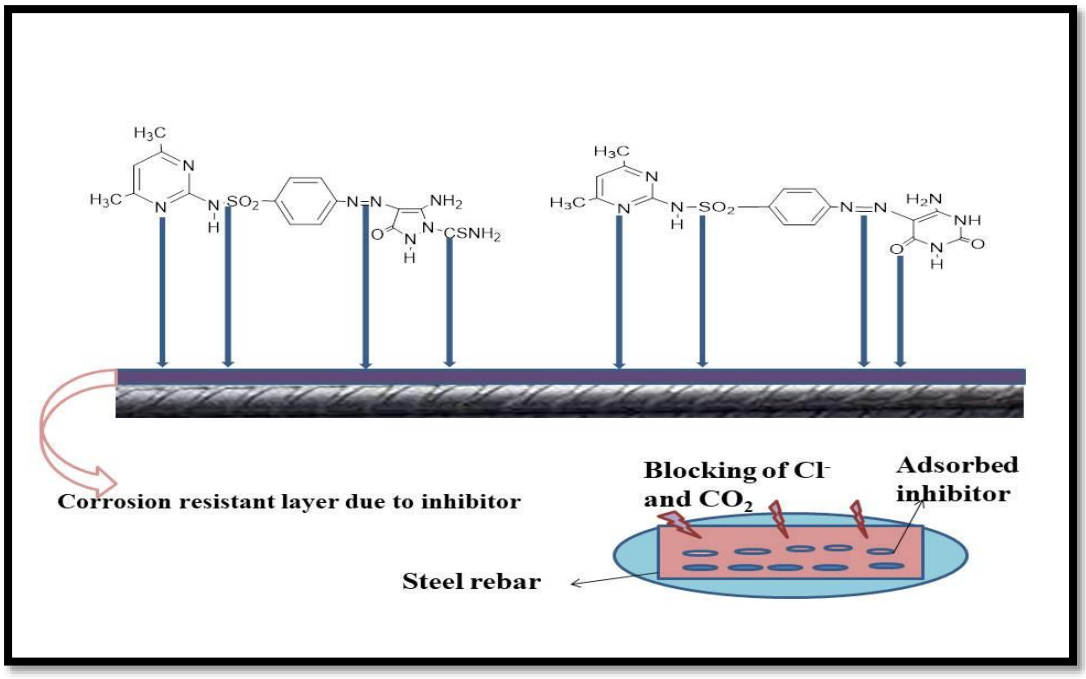


**Fig. 4.19(b): Schematic representation of mechanism of rebar corrosion in presence of synthetic inhibitors**